Journal of Polymer Science

WILEY

JOURNAL OF POLYMER SCIENCE

RESEARCH ARTICLE OPEN ACCESS

Performing Polarized Raman and Digital Image Correlation Analysis to Understand the Increased Ductility of Microscale Epoxy Materials

Janina Mittelhaus[1] | Julius Jacobs[1] | Suprit Bhusare[2] | Nazanin Pournoori[2] | Matti Isakov[2] | Turkka Salminen[3] | Holger Schmalz[4] | Gaurav Mohanty[2] | Essi Sarlin[2] | Bodo Fiedler[1]

[1]Hamburg University of Technology, Institute of Polymers and Composites, Hamburg, Germany | [2]Tampere University, Faculty of Engineering and Natural Sciences, Materials Science and Environmental Engineering, Tampere, Finland | [3]Tampere University, Microscopy Center, Tampere, Finland | [4]University of Bayreuth, Macromolecular Chemistry and Bavarian Polymer Institute, Bayreuth, Germany

Correspondence: Janina Mittelhaus (janina.mittelhaus@tuhh.de)

Received: 21 October 2024 | **Revised:** 11 February 2025 | **Accepted:** 11 February 2025

Funding: This work was supported by Deutsche Forschungsgemeinschaft (DFG, German Research Foundation) (525597740). G.M. and S.B. acknowledge partial funding from project DURATRANS (364408, 2024–2027, under the framework of M-ERA.Net) and HERBIE (341050, Research Council of Finland). Publishing fees are supported by the Funding Programme Open Access Publishing of Hamburg University of Technology (TUHH).

Keywords: DIC | epoxy films | polarized Raman microscopy | shear bands | strain hardening | strain softening

ABSTRACT

The highly cross-linked (epoxy) matrix material in fiber reinforced polymers has a microscopic volume between fibers and therefore exhibits different mechanical behavior in comparison to standard bulk epoxy samples. It has been found in previous studies that a decreased epoxy gauge volume leads to an increased deformation ability (necking and shear band formation). By using laser cutting to create dogbone samples from manufactured epoxy films, the gauge volume can be further reduced in comparison to previous studies, and the ductility can be enhanced even further. To understand load-induced molecular mechanisms responsible for the increase in ductility at macroscale, this study combines digital image correlation (DIC) with tensile tests and precise force measurement. The global and local strains are calculated using the DIC data. The determined strains reach values up to 80% (global strains) and 120% (local strains), respectively. These strain values are significantly higher than those of archetypical brittle epoxy bulk samples (less than 10%). Polarized Raman spectra show that load-bearing backbone molecules in the deformed film sample regions are oriented in the tensile load direction. This orientation might be due to the unraveling of entanglements, which can be seen as a sudden decrease followed by a subsequent rise in engineering stress values during deformation.

1 | Introduction

Fiber reinforced polymers (FRPs) can often be found in industrial applications that require excellent mechanical performance at low weight, for example, in aviation or automotive industry. The structure of FRPs consists of oriented fibers surrounded by a continuous matrix material, such as an epoxy resin system. This results in a structure with areas of matrix materials that are in the (sub) micrometer range, such as resin-rich zones between fibers ($1-25\ \mu$m, intralayer) and between reinforcing prepregs or layers ($10-200\ \mu$m, interlayer) [1]. The standard characterization of matrix materials is usually performed using macroscopic test volumes such as those specified in the standardized test methods ASTM D638 and DIN EN ISO 527. Accordingly, when modeling FRPs, it is often assumed that the epoxy-based matrix, has bulk mechanical properties. Using the

bulk mechanical parameters of standard specimens as input for microscale modeling of composite materials can lead to insufficient agreement between the modeled and experimentally observed behavior [1–4]. Beside geometrical constraints, this might be due to the deviation of the mechanical behavior of the microscopic matrix from the macroscopic standard bulk specimens. It has been shown in previous studies that the ductility and plasticity of an archetypical brittle epoxy matrix can be increased by reducing the gauge volume [1, 5–7]. Especially microscale epoxy films exhibit an increased deformation ability due to necking and the formation of shear bands under tensile load [8]. However, to date, there is no complete physical, mechanochemical or molecular explanation for the observed size effect regarding the deformation ability and the mechanisms behind the shear band formation. The knowledge about this can further help to optimize the mechanical behavior of FRPs since the matrix deformation potential significantly affects the overall mechanical behavior of FRPs. For even more accurate modeling and design of FRPs, the mechanical behavior of epoxy should not be based on the mechanical parameters of bulk samples, but on the parameters of microscopic epoxy samples in order to improve the accuracy of micromechanics-based models.

For film samples, with a comparably small gauge volume, a very sensitive load cell and a suitable micro tensile test device are necessary to investigate the mechanical behavior. Performing tensile tests with an appropriate setup will allow accurate measurement of changes in force (stress) due to molecular processes inside the epoxy material.

The strain analysis can be done by applying the digital image correlation (DIC) technique, where the (surface) deformation of the test specimen is observed during the test based on tracking a random speckle pattern on the sample surface. This approach has been used for several FRPs with epoxy matrix [9–14] to analyze the interphase region between the matrix and fibers and to correlate the local deformation mechanisms with the macroscopic mechanical parameters.

To investigate the molecular processes, which lead to the local and global mechanical response to external stress, Raman spectroscopy can be used. In particular, polarized Raman spectroscopy allows the analysis of polymer backbone orientations [15–19]. The technique is usually applied to semi-crystalline polymer films, surfaces, and fibers, like poly(ethylene terephthalate) [20–23], polyethylene [24] and polypropylene [25]. In this study, polarized Raman measurements were performed on the shear bands and the deformed regions of the tensile-loaded epoxy film specimens. The purpose was to analyze the molecular changes and associated local deformations in these regions. This facilitates the observation of the presumed unraveling of entanglements, molecular alignment, and bond stretching due to the applied tensile load.

A combination of these methods will provide a detailed insight into the micromechanical properties of the thermoset matrix as a micro-component of composites. This is important for the optimization of the design and performance of polymeric composites with an epoxy matrix. Furthermore, as the multiscale modeling of composite materials becomes even more popular and essential for the industry, it is necessary to fully understand the required conditions for the increased deformation ability and the underlying mechanisms in epoxy.

Therefore, in this study, a combination of microscale tensile tests with DIC followed by photoelastic imaging and polarized Raman analysis of the deformed film specimen is used to visualize the deformation and to understand the associated molecular backbone movements and orientation as a result of the applied tensile load.

For this study, a low viscosity resin has been chosen to produce thin epoxy film samples with a previously developed manufacturing method [8]. The samples, which had a dogbone geometry with a comparably small gauge volume, were cut by a femto-second laser from the thin epoxy films.

2 | Materials and Methods

A low viscosity resin system consisting of EPIKOTE Resin MGS RIMR 135, which is based on diglycidyl ether of bisphenol A (DGEBA), combined with a liquid aliphatic diamine hardener, EPIKURE Curing Agent MGS RIMH 137 (Westlake, International: USA/Europe) was used. Both components were mixed in a weight ratio of 100:30 in a mixer (SpeedMixer DAC 150.1 FVZ) at 3500 rpm for 5 min. The backbone of the DGEBA is shown in Figure 1.

2.1 | Epoxy Film Samples

In a previous study, a new liquid molding process was developed and optimized to produce thermoset films with a defined thickness [8]. By using this manufacturing method, epoxy films with thickness of $30.36 \pm 2.01\,\mu m$ were created for this study. After the fabrication, the selected thickness of the films was verified with a dial gauge and the utilized dogbone geometry (see Figure 1) was created by femto-second laser cutting from defect free film regions (confirmed via microscopy analysis). A laser with a wavelength of 343 nm and a beam size (in focus) of approximately 10 μm was used. The cutting speed was set to 175 mm/s which amounts to pulse energy of 4.6 μJ. The geometric dimensions of the cut dogbone samples deviate

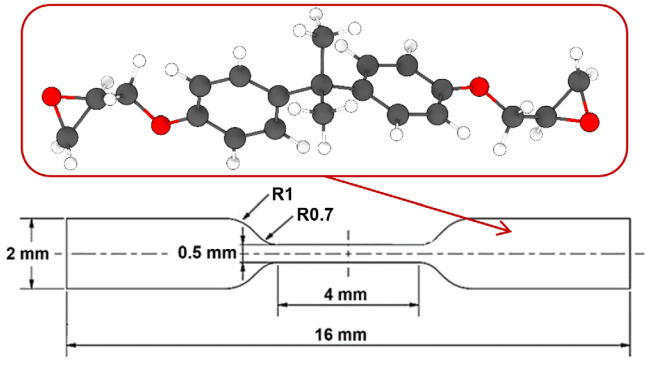

FIGURE 1 | Dogbone sample geometry for tensile test with a gauge volume of 0.06 mm^3 and the chemical structure of the DGEBA backbones.

from the established standard DIN EN ISO 527-3, as they are predefined by the used microtest grippers for the tensile tests and the gauge volume is further reduced in comparison to the previous studies [8], due to limitation in maximum force of the load cell. The gauge length was 4 mm and the gauge volume was about 0.06 mm^3 for the chosen dogbone specimen geometry.

2.2 | Tensile Test and DIC Analysis

An Alemnis in situ nanoindenter was modified with grippers to perform tensile tests. Alemnis sample-side load cell (SLC-2.5) was used. This load cell has a load range of 2.5 N and load resolution of $< 15\ \mu$N. All experiments were confined to loads less than 2 N. The displacement was applied using the Z stage of the nanoindenter, which is based on piezoactuation mechanism and has a resolution < 10 nm. The compliance of the nanoindenter setup for the micro tensile tests was found to be 4.3 nm/mN.

All tensile tests were performed in displacement-controlled mode at room temperature. The compliance was taken into account during the mechanical data evaluation. A displacement rate of 0.3 mm/min was imposed resulting in a nominal strain rate of $10^{-3}s^{-1}$ to provide the epoxy material with sufficient time to undergo the (molecular) deformation processes. In total, six samples (three longitudinal and three transverse to the resin flow direction in the film manufacturing process) were tested with this setup. Supplementing the standard series of tensile tests, a second set of tensile tests on six further samples was carried out using the DIC analysis to obtain information about local strains. In preparation for these tests, a fine stochastic speckle pattern was applied onto the epoxy film samples using black spray paint. The spray paint was sprayed against a plastic disk in an approximately 45° angle where the spray paint bounced off and fell onto the samples which were horizontally placed on a paper. It should be noted that the DIC paint was not applied as a continuous layer, thus, the mechanical response should be similar to the previously tested samples without paint and the influence of the color particles is, therefore, considered negligible.

After the applied color had dried, the pattern was checked for DIC applicability under an optical microscope. The samples with a feasible speckle pattern were tensile tested combined with DIC immediately after the pattern application. For this purpose, the loading stage with the clamped sample was positioned under a stereo-optical microscope from Leica with a camera and a USB connection for video and images storage. The magnification was set so that optical resolution of $\sim 10\ \mu$m/pixel at the gauge section was achieved. The DIC system was calibrated using a calibration plate (a glass plate with rectangular grid of dots placed at 0.5 mm from each other). During the mechanical loading of the samples, a video with 15 frames per second were recorded. The duration of the tensile tests varied from 300 to 515 s resulting in >4500 frames collected per tested sample. For the DIC analysis and results presented in this study, every 100th image was used resulting in an effective frame rate of 0.15 frames per second or 6.67 s between the frames, which is considered sufficient for the present purposes. The DIC analysis was performed with LaVision DaVis 10.2.1 software with the following correlation parameters: correlation relative to first frame, 2nd order shape functions and subset size/step size ranging from 19/6 to 23/7 pixels. It is noteworthy that due to the evident challenges related to the creation of the speckle patterns in such a small length scale, the resulting pattern speckle size was not homogeneous as highlighted by the example in Figure S1. Most speckles were less than 10 pixels in size, the smallest being in the 3–5 pixel size, which is considered optimal [26]. However, there were also some notably larger speckles (up to 30 pixels). In order to obtain sufficient spatial resolution, the subset and step sizes were selected based on the smaller speckles. This choice led to some loss of data at the vicinity of the larger speckles and in areas with lower local speckle density; this loss was deemed acceptable in the present work.

The resulting deformation data were analyzed in terms of strain fields obtained directly from the calculations as well as in terms of data obtained via post processing, that is, virtual extensometer and strain along a line placed longitudinally on the gauge section. The DIC data were additionally used to check the global engineering strain determined via the displacement of the *Z*-stage of the nanondenter based on the piezoactuation mechanism. The determined and measured global strain values were found to be almost identical.

2.2.1 | Polarized Raman Spectroscopy

The polarized Raman spectroscopy measurements were performed with a Renishaw inVia Qontor Raman microscope using a 50x long working distance objective (NA 0.55). The laser wavelength was 532 nm and the spectrometer had a grating with 1200 grooves per millimeter (spectral resolution of 2 cm^{-1}). The resolution was 0.5 μm in *X*- and *Y*-direction. Before mechanical testing, the six film samples (without DIC pattern) were analyzed in the as-produced state to identify the initial molecular state.

Therefore, Raman spectra at four different sample positions in the gauge length were recorded. For every measurement position, the measurements were performed in polarization along the load direction (*X*) and perpendicular to the load direction (*Y*) for 120 s (see Figure 9). After mechanical loading and final failure, Raman spectra were recorded in both polarization modes in the macroscopically deformed sample regions with shear bands and reduced cross-sections, and in the undeformed sample regions. The raw data were processed by cosmic ray removal, and the background was corrected using a 4th order polynomial.

Additional measurements were done using a confocal WITec alpha300 RA+ Raman imaging system, equipped with a UHTS 300 spectrometer (grating: 600 groves/mm) and a back-illuminated Andor Newton 970 EMCCD camera together with the WITec Suite SIX 6.1 software package. Measurements were conducted with the same laser wavelength as described above, employing a 50× long working distance objective (Zeiss LD EC Epiplan-Neofluar Dic 50x, NA 0.55), a typical laser intensity of 22 mW (integration time 0.5 s, 50 accumulations). All spectra were subjected to a cosmic ray removal routine and baseline

correction (shape mode) implemented in the WITec Project SIX 6.1 software.

2.3 | Photoelasticity

In addition to mechanical tests and spectroscopic investigations, photoelasticity was used as a further supplementary method after mechanical loading. With the use of polarized light, the stress distribution in the translucent epoxy films could be studied.

For this purpose, a Keyence VHX-6000 microscope was used together with a VH-Z20 objective and polarization adapters after mechanical loading.

Two different polarization filters were used. These two polarizing filters were aligned in 90° to each other. The measurement was performed in transmitted light mode, that is, the translucent and deformed epoxy film was positioned on a glass specimen holder between the two polarizing filters, which allowed an analysis with cross-polarized light.

3 | Results and Discussion

3.1 | Tensile Testing

No significant differences between the mechanical behavior of samples cut longitudinal or perpendicular to the resin flow direction could be observed. Figure 2 shows representative engineering stress–strain curves of longitudinal and transverse epoxy film specimens without a DIC pattern. The global strain was determined from the crosshead (*Z*-stage) displacement which is based on piezoactuation. Unless explicitly stated otherwise, the global strain in this study was always determined in this way. The elongation at break is 83% and the tensile strength is about 54 MPa for the longitudinal sample 1 and 82% and 54 MPa for the transverse sample 1. The general mechanical parameters for the samples tested without the DIC pattern is about 77.3% ± 6.1% for the elongation at break and 52.0 ± 2.8 MPa for the tensile strength. The latter is reduced compared to previous film sample geometries [8], but the global strain at break is remarkable for an archetypal brittle epoxy material and is significantly increased compared to standard bulk samples (less than 10%) and other epoxy film samples with a larger test volume [8]. After yielding, the engineering stress decreases and strain softening takes place.

Especially for the longitudinal sample this can be seen around global strains of 32%, 52%, and 72% (see Figure 2 the black arrows), the stress decreases followed by an increase (strain hardening) with further tensile deformation. This type of behavior can be found also for epoxy volumes tested under pure shear [27], but not for standard bulk samples in tension [28]. This macroscopic strain softening and hardening might be explained as follows. The global stress decreases due to the presumed unraveling of entanglements and molecular alignments inside the material. After the stress is partially relaxed by the molecular movements and macroscopically visible shear bands are formed in some sample areas, the stress increases again due to the hardening effect of the molecule chains aligned in the tensile direction inside the deforming sample. Strain softening and hardening can be found for example in glassy thermoplastics [29, 30] or some amorphous thermosets under compression load [31]. To the knowledge of the authors, strain softening and hardening with accompanying formation of shear bands for neat epoxy has so far only been observed sporadically in compression tests and tensile tests at elevated temperatures [32], but not yet for tensile tests at room temperature. In the study of Sui et al., microscale epoxy fibers having a gauge length of 10 mm and diameters between 30 and 120 μm exhibited strain softening and hardening under tensile load, but shear bands were not observed in these necked fibers [6].

3.2 | Photoelasticity and DIC

The shear bands and the reduced widths of the specimens can be visualized in photoelastic digital microscope images, as can be seen in Figure 3 for two representative epoxy film samples after

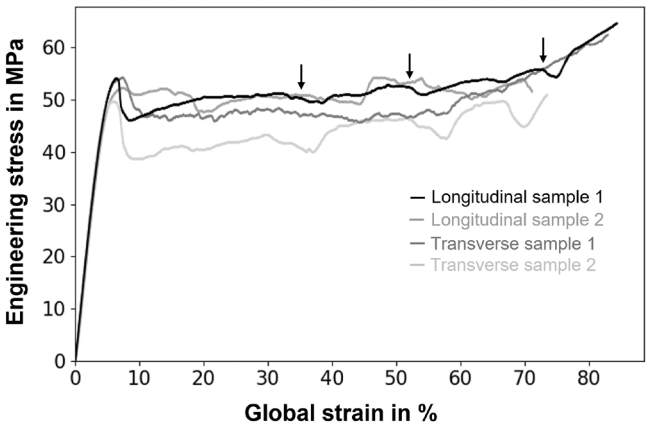

FIGURE 2 | Representative engineering stress–strain curves of two longitudinal and two transverse (to the resin flow direction) cut epoxy film specimens. Stress decreases for one longitudinal sample (black curve) are marked with black arrows.

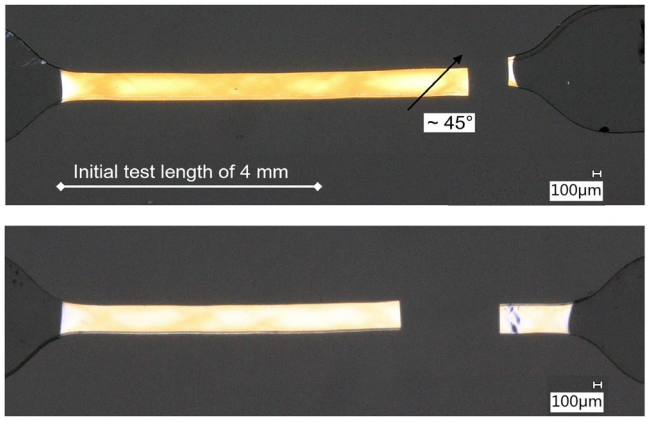

FIGURE 3 | Photoelastic images of deformed epoxy film samples after tensile testing (elongation at break of 74% [top] and 71% [bottom]). The initial gauge length is marked and shear band structures in 45° to 55° are visible. The different yellow colors represent mechanical stresses in the material.

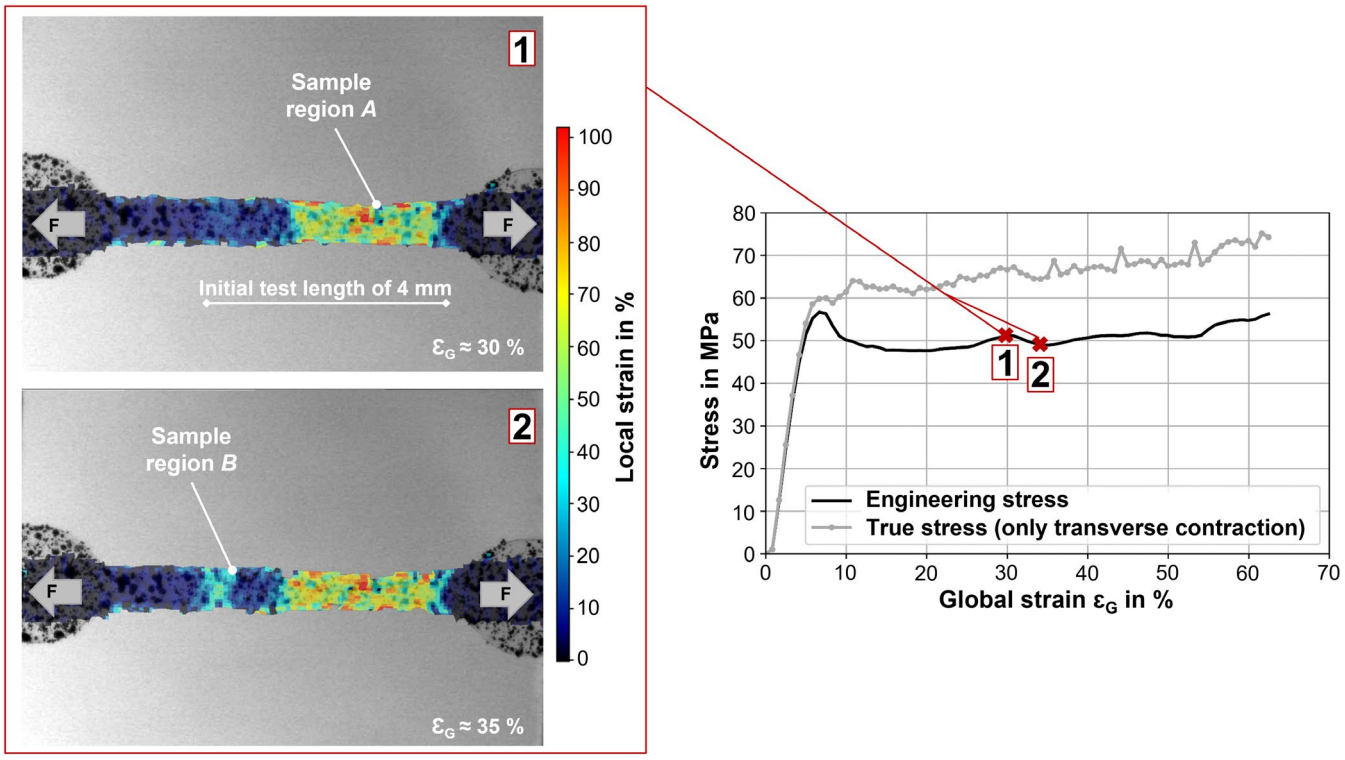

FIGURE 4 | Visualized DIC data at a global strain around 30% (image 1, top) and 35% (image 2, bottom) and the corresponding engineering stress–strain curve (black) and true stress–strain curve (gray, only maximal transverse contraction in the gauge length from the DIC data) of a representative epoxy film sample. The DIC field data are shown by colorized quadrilaterals so that the subset size used in the calculation corresponds to $3 \times 3 = 9$ quadrilaterals in this figure.

tensile testing. The yellow regions indicate mechanical stresses within the epoxy samples.

The shear band orientation of 45°–55° to the tensile direction and reduced gauge width can also be seen in the DIC deformation field data shown in Figure 4 (left). As described, after the peak yield stress is reached, the sample does not deform uniformly. Here, a distinct deformation can be seen on the right-hand part (region *A*) of the sample gauge section (see Figure 4 (left, 1)). The maximum local strain reaches values of up to 100%. The local deformation phenomena are also evident in the global engineering stress–strain curve, as can be seen in Figure 4 (right). During the formation and growth of local deformation region *A*, the stress remains relatively constant. After a specific level of molecular orientations in the tensile direction has been reached, strain hardening takes place, and the stress increases as the aligned molecular backbones are further stressed and stretched. The stress maximum for the deformation region *A* is approximately at 30% global strain. When a global strain around 35% is reached, increased local strain values are detectable in sample region *B*, where a second shear band formation within the gauge length begins, as can be seen in Figure 4 (left, 2). This correlates with a decrease in global stress since the external mechanical energy is used for the molecular backbone movement processes, as can be seen in the corresponding engineering stress–strain curve (strain softening). The second deformation zone probably appears because the maximum possible amount of deformation for the first deformation region *A* and the required yield stress for a second deformation zone is reached in the left sample side around region *B*. Thus, the formation of a new deformation on the left-hand side of the specimen (region *B*) is energetically more feasible than continued deformation in the first zone (region *A*), where hardening resulting from local molecular reorientation has already taken place. At the end of the tensile test or before final failure, a large part of the sample gauge length is deformed, that is, most of the backbone chains are oriented, and the stress increases again. To take the width reduction into account, the true stress–strain curve for the same sample was determined based on the local maximum contraction in the transverse direction within the gauge length for each time increment. However, it is not possible to include possible load-induced thickness changes in this method. This is why the initial thickness is taken for this procedure.

The true stress curve is also shown in Figure 4 (right). Since the measured contraction in the transverse direction depends on the quality of the DIC pattern, the true stress–strain curve contains some peaks or fluctuations. The overall trend shows increasing stress values after reaching the yield stress since the true cross section decreases due to the reduction in widths. Nevertheless, in the true stress curve, the aforementioned peaks of strain hardening and strain softening are still visible at the same global strain values.

The DIC data of the presented film specimen in Figure 4 were further analyzed regarding the strain softening and hardening effects. A detailed DIC investigation was performed where different sections along the gauge length of 4 mm were compared to each other. This is visualized in Figure 5. The *y*-axis in the graph (see Figure 5, right) shows the global strain or the progress

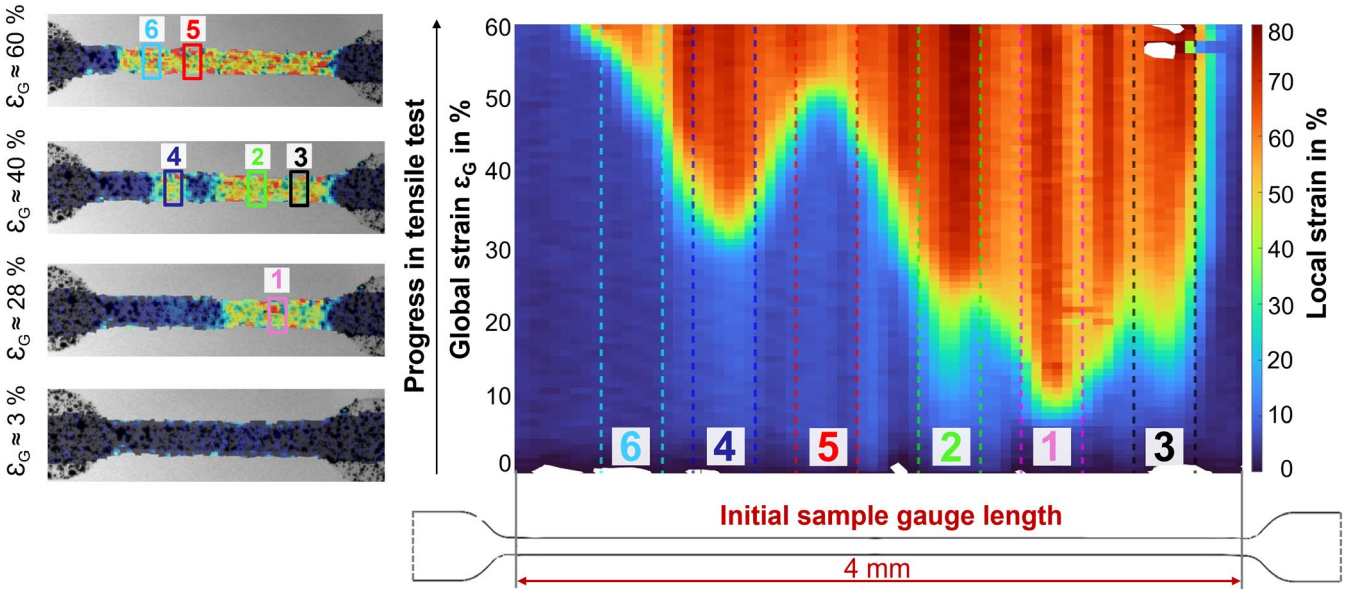

FIGURE 5 | Visualized DIC data including the local strains, which are colored regarding the corresponding strain values during the tensile test (global strain) for selected sample positions in the initial gauge length.

in tensile test, that is, it is a temporal axis. By assigning the local strain values to a color scale, it was possible to visualize and determine the local strains for each selected specimen position at each time point (or global strain value) during the tensile test.

The sample positions and assigned numbers were selected regarding the beginning of an increase in the local strain values (as indicated in Figure 5). At the beginning of the tensile test in the elastic and viscoelastic region, that is, at low global strains, there is no reduction of the widths or high local strain values detectable (with the used color scale, the entire gauge length is blue). At sample position 1, the local strain increases, deformation and shear bands start and grow in the direction of positions 2 and 3 as the tensile test progresses. In these sample regions, the local strain values increase further as the tensile test progresses.

As mentioned before (see Figure 4), at a global strain around 35%, a second deformation zone is created at position 4. This deformation zone extends in the direction of positions 5 and 6. At the end of the tensile test or shortly before the final failure, the entire gauge length has reduced width except for a small sample region on the left side next to position 6. The local strain curves at these six selected specimen positions over the progress of the tensile test are displayed in Figure 6. The local strain values were calculated for each time as an average local strain across the sample width. It can be seen that the strain curves for all selected sample positions follow a similar pattern. In the beginning of the tensile test, there are only moderate local strain values and a slight gradient due to the elastic and viscoelastic behavior of the epoxy. As the tensile test progresses, a steep increase in local strain is first observed at position 1. Here, the strain increases up to a maximum local strain value of approximately 60%, and the local strain value remains almost constant afterward. When reaching the constant strain value in position 1, the local strain in position 2 starts to increase, as well as in position 3 since the deformation grows in both directions. In the same way, it can be seen that the local strain of position 5 rises sharply when the

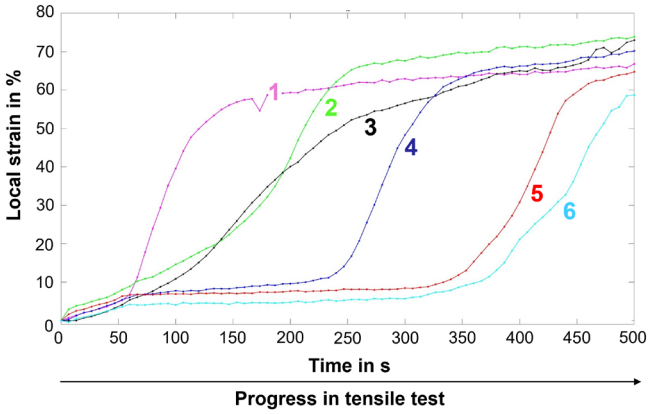

FIGURE 6 | Local strain curves for six selected locations on the initial gauge length over the tensile test duration (see Figure 5).

local strain in position 4 is reaching the constant or maximum value. The difference in the local strain histories for positions 5 and 6 is minor as the deformation grows from position 4 in both directions (toward positions 5 and 6). These results imply that at the microscopic level, after a sufficient stress level is reached, the backbones can be oriented and stretched inside the epoxy material until a characteristic threshold (local strain around 60%) is reached. Stretching may include the increase of load-bearing bond lengths and a more linear conformation.

Afterwards, it seems to be energetically more favorable to continue the deformation process in another region of the sample, where the local yield stress is reached.

3.3 | Polarized Raman Microscopy

The *X* (in load direction) and Y (transverse to load direction) polarized Raman spectrum of an unloaded or as-produced

epoxy film sample are shown in Figure 7. The initial polarized Raman spectra show no polarization dependent intensity or differences between the *X* and *Y* spectra, which means that no molecular orientation from the film manufacturing process is evident. This is in line with the mechanical data of the transverse and longitudinal samples, which show no significant differences.

Between the *X* and *Y* spectra of undeformed sample regions of a loaded epoxy film sample, there is no significant difference as well as (see Figure 9b).

To visualize the differences between the deformed and undeformed regions of the samples in more detail, a mapping in *X* and *Y* polarization modes was performed. The map data was processed with k means cluster analysis to identify regions with similar spectra. In Figure 8, it is clearly visible that the *X* polarized spectra differ between the two regions, that is, deformed (left) and undeformed (right). This is highlighted with two different colors (blue and cyan). Each color represents almost similar spectra for the corresponding measurement points. Since the Raman method does not depend on the sample thickness like Infrared spectroscopy, the reduction of the thickness can be excluded as the cause of the spectral differences.

Each pixel represents one measurement point. All blue pixels (deformed) and all cyan pixels (undeformed) have similar spectra. The averaged spectra of both regions in *X* polarization mode are shown.

Further Raman analysis shows that the polarized spectra recorded after the tensile test show increased intensities of the *X* polarization mode (in tensile direction) in the deformed sample with reduced widths (see Figure 9a).

At the same measuring positions, comparably lower intensities for the *Y* polarization mode (perpendicular to tensile direction) are detected for most peaks, as can be seen in Figure 9. This is especially evident for the molecular backbone components, as for the different aromatic vibration modes (peaks at 1605, 1580, 1105, and 821 cm^{-1}) [33, 34], which exhibit a significantly increased intensity for the *X* polarization in load direction. Even though generally a normalization is applied when comparing spectra, this was deliberately omitted here in order to show the

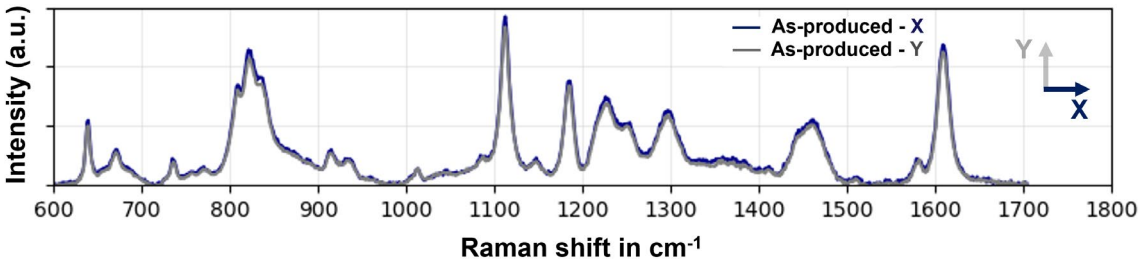

FIGURE 7 | *X* and *Y* Raman spectrum of an as-produced epoxy film sample. Both spectra are recorded at the same sample position.

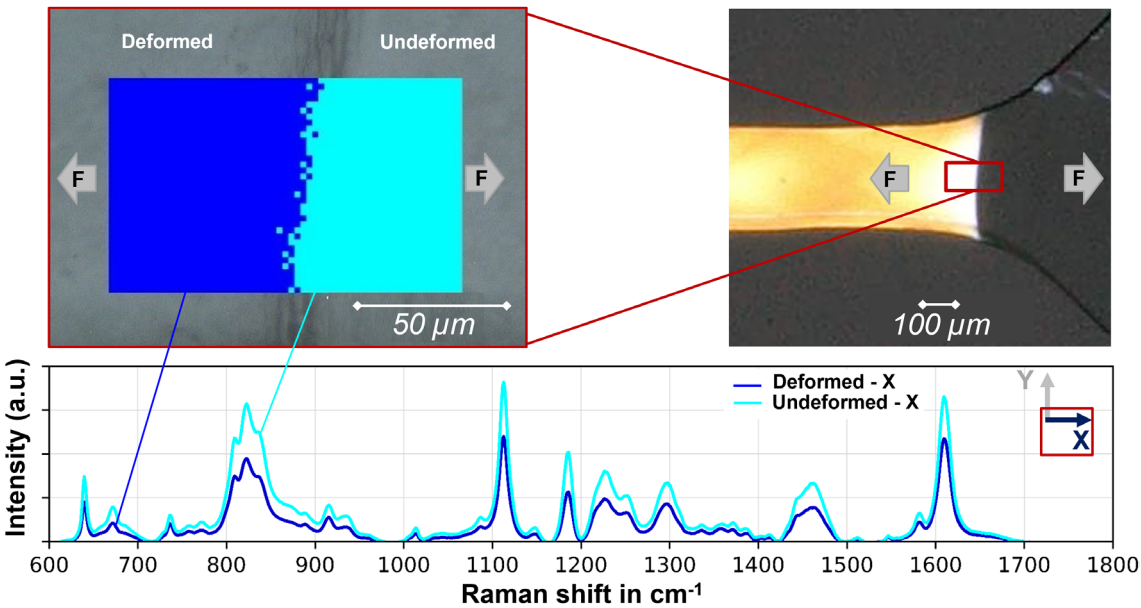

FIGURE 8 | Mapping and k-means cluster analysis in *X* polarization mode over the interface between the deformed (left) and undeformed region (right) as shown in the corresponding photoelastic image (right). The sample was stretched until a global strain $\epsilon_G = 73\%$. The cluster analysis was performed using the Renishaw Wire software. The initialization was chosen as random and the clustering type was k-means, using correlation as the distance metric. The initial number of clusters was chosen as five, but based on the similarity within the spectra of the identified clusters in different regions, the final number was reduced to two.

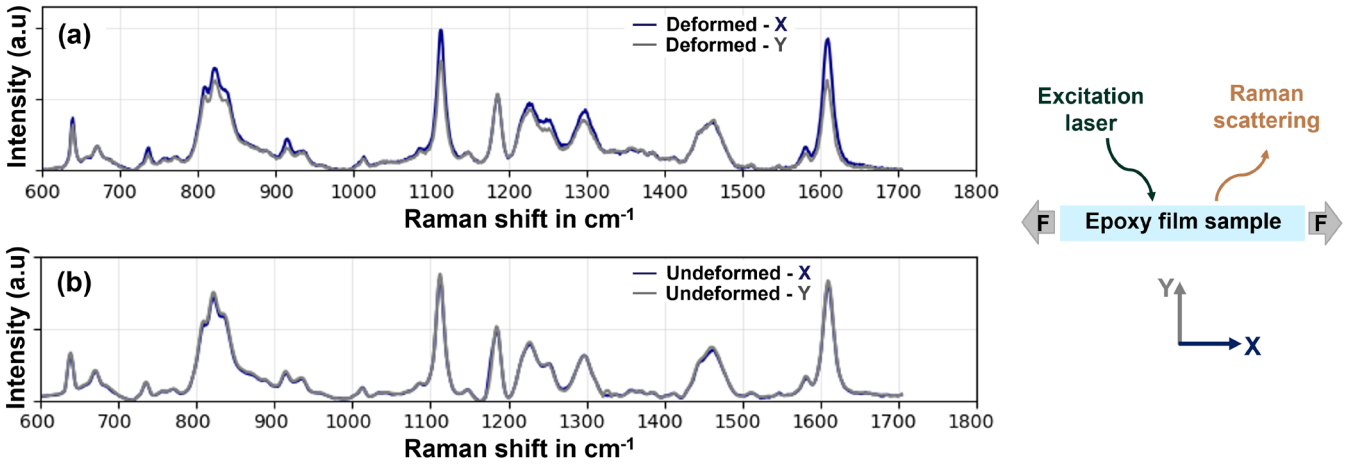

FIGURE 9 | Polarized Raman spectra of a tensile tested epoxy film sample. (a) Spectra for two different polarization modes (*X* and *Y*) in a deformed sample region with shear bands and (b) pictured the spectra (*X* and *Y*) recorded in an undeformed sample region. The polarization directions are shown with regard to the tensile direction.

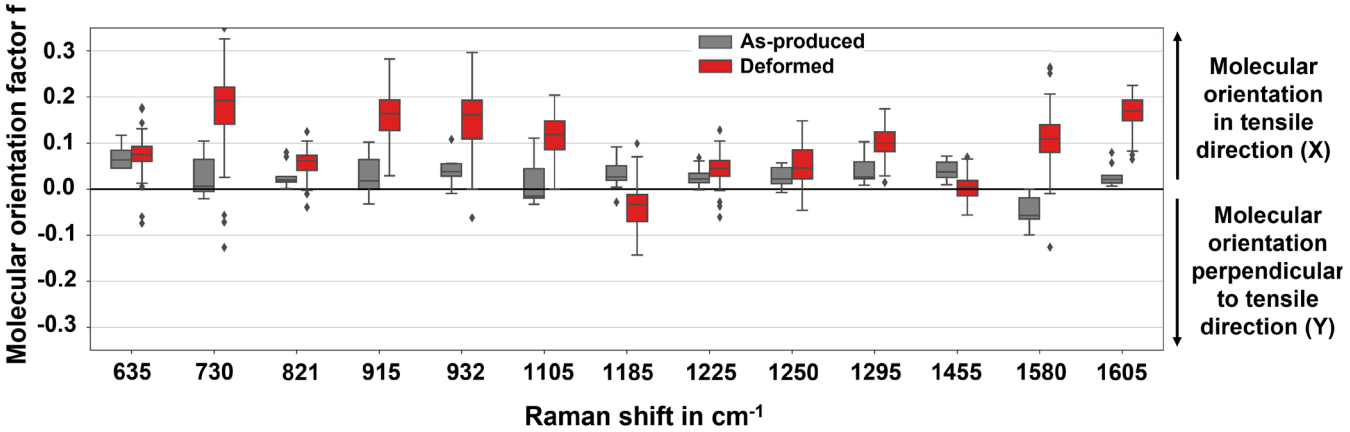

FIGURE 10 | The molecular orientation factor is shown as a box plot for each Raman peak from the deformed sample region and the as-produced initial sample state. The factor is determined from Equation (1) with the *X* and *Y* polarized intensity.

differences for all peaks. The data processing was therefore carried out exclusively as described in Section 2.2.1.

Another way to demonstrate molecular orientations is to determine the molecular orientation factor *f* for each peak as follows:

$$f_{\text{Peak}} = 1 - I_{Y,\text{Peak}} / I_{X,\text{Peak}} \quad (1)$$

I refers to the intensity of the corresponding Raman peak, where *X* and *Y* indicate the polarization mode with regard to the tensile direction.

The factor *f* is not an absolute value of molecular orientation, but can be used for comparative studies [5, 35]. Note that the factor *f* varies from 0 to 1, corresponding, respectively, to random and perfect alignments parallel to the tensile direction (*X*). However, it could take a negative value if the molecule has preferred orientation in the transverse direction (*Y*). The molecular orientation factor for all peaks were determined and is shown as box plot in Figure 10. The peaks corresponding to backbone segments exhibit a positive value for the molecular orientation factor, which means an orientation of the corresponding molecular segments in load direction. Only the peaks at 1455 and 1185 cm^{-1} exhibit a negative molecular orientation factor.

The peak at 1185 cm^{-1} corresponds to the in-plane stretching vibration of *gem*-dimethyl group of bisphenol A between the aromatic rings and the peak at 1455 cm^{-1} is related to the methyl and methylene vibrations (see chemical structure in Figure 1) [5, 34, 36]. Both peaks correspond to molecules that are not directly part of the backbones. In addition, the aforementioned side bonds are almost perpendicular to the backbone [5]. If the backbones get oriented in the tensile direction (*X*), these bonds are increasingly aligned perpendicular to the tensile direction (*Y*).

The fact that molecular orientations can only be found in severely deformed sample areas can be seen visually again in Figure 11.

At different selected sample positions within the gauge length (marked as gray dots in Figure 11a), Raman spectra in *X* and *Y* polarization direction (I_X, I_Y) were recorded and used for the calculation (see Equation 1) of the molecular orientation factor of the peak at 1605 cm^{-1}, which corresponds to in-plane C—C

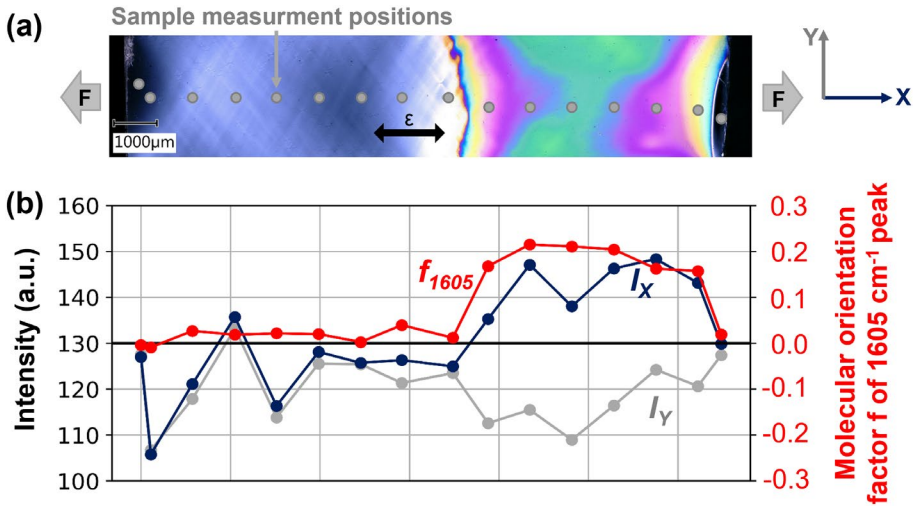

FIGURE 11 | Photoelastic image of a deformed epoxy film sample (global strain $\epsilon_G = 17\%$) with white colored shear bands and yellow, purple and green colored mechanically stressed and deformed sample region (a) and the molecular orientation factor (red line) determined for the aromatic peak at 1605 cm^{-1} (b) for different sample positions (marked as gray dots in photoelastic image) in the gauge length. The corresponding intensities of the aromatic peak at 1605 cm^{-1} for each sample measurement point for the X (I_X) and Y (I_Y) polarized measurements are shown as well (gray and dark blue lines).

stretching vibrations in the aromatic rings. The calculation results are shown in Figure 11. The experimental evidence leads to the conclusion that in highly deformed sample regions with shear bands (white shear bands and yellow, purple, green colored and mechanically stressed sample region in the photoelastic image in Figure 11a), the backbones with the aromatic rings are oriented in tensile direction. As a component of the backbones, the aromatic rings or *para*-phenylene groups are directly involved in the load transfer. High local strain values in the shear bands indicate that the molecular bonds within the material are stressed and stretched in these sample regions. This is consistent with previous studies that have indicated that the *para*-phenylene groups, as a load-bearing part of the backbones, might be stretched as an IR redshift is detectable [8] and a molecular environment change can occur in microscale epoxy samples [37]. In this study, it was possible to show that the backbones within the shear bands of deformed epoxy film samples are also aligned in the tensile direction.

The study by Sui et al. [5] on necked epoxy fibers has shown that the side chains of the backbones are oriented perpendicular to the tensile direction and it was assumed that the backbones might be aligned in the tensile direction. This is in line with the results presented here and the evidence that the backbones are oriented in the tensile direction.

4 | Conclusion

It has been shown that with an essential decrease of the test volume of epoxy samples, the deformation ability and elongation at break (up to 85%) in tensile tests increase significantly and are remarkable for an archetypical brittle thermoset material, especially compared to standard bulk epoxy specimens. Shear bands and regions of reduced widths are clearly visible in the photoelastic images after tensile tests and final failure. The tensile test data with a very precise force recording and local strain determination via DIC show an interplay of stress increase and decrease, macroscopic growth of deformation zones, and formation of shear bands.

The molecular processes such as unraveling of entanglements, molecular backbone stretching, and alignment might lead to a decrease of stress and strain softening. After the alignment of molecular backbones in the load direction and local strain values up to 100% are reached, a stress increase and strain hardening are recognizable in the engineering and true stress–strain curves.

With a detailed DIC analysis, it was possible to show that after reaching a characteristic local strain level in a deformation zone, a new deformation localization takes place in neighboring regions. The deformation grows over the entire sample gauge length until the molecular backbones within the network or material cannot be further oriented due to spatial hindrance of neighboring molecules. At this point, final failure may occur due to multiple molecular chain scissions.

Polarized Raman measurements showed that the molecular backbones are oriented and aligned in the load direction only in the deformed sample regions, which means that high local strain values appear with shear bands and molecularly oriented backbones. This allows the conclusion that at low strain rates for samples with microscale gauge volume, it is possible to reach high ductility and increased elongation at break as a result of molecular movements, even in a high-crosslinked epoxy material.

Further experimental studies on epoxy films and epoxy simulations are planned in order to understand the molecular processes in detail and to gain an even better understanding of the necessary requirements for the increased ductility. A further gauge volume decrease even closer to the often appearing epoxy matrix volume in FRPs by guaranteeing an accurate and optimized sample handling would allow an even more realistic analysis of the deformation ability under external load in epoxy matrix regions in FRPs. By better understanding the described interactions

between macroscopic ductile deformation behavior, the formation of shear bands, and the associated molecular structural changes, the aim is to enable more accurate modeling and improved composite development in the future.

Acknowledgments

The research was done in collaboration with Tampere University and Hamburg University of Technology (Institute of Polymers and Composites) and the research strategy was a result of joint efforts. During the collaboration, J. Mittelhaus completed a 2 months' research visit at Tampere University funded by DAAD (German Academic Exchange Service). Before the visit, the epoxy film samples were manufactured at TUHH (Prof. B. Fiedler, M.Sc. J. Mittelhaus, M.Sc. J. Jacobs, M.Sc. P. Röttger). At Tampere University, there were two research groups involved in the work and a large group of scientists: the research group for Plastics and Elastomer Technology (Assoc. Prof. E. Sarlin, Dr. P. Laurikainen, M.Sc. N. Pournoori) and the Multiscale Mechanics of Materials Research Group (Asst. Prof. G. Mohanty, M.Sc. S. Bhusare), as well as Dr. T. Salminen from Tampere Microscopy Center and Dr. M. Isakov from Materials Science and Environmental Engineering. This work made use of H2MIRI and Tampere Microscopy Center research facilities at TAU. Dr. H. Schmalz supported the research by performing polarized Raman measurements at the University Bayreuth. We acknowledge support from the keylab "Synthesis and Molecular Characterization" of the Bavarian Polymer Institute (BPI) at the University of Bayreuth. This research at TUHH received funding from Grant No. 525597740 provided by the Deutsche Forschungsgemeinschaft (DFG, German Research Foundation). G.M. and S.B. acknowledge partial funding from project DURATRANS (364408, 2024–2027, under the framework of M-ERA.Net) and HERBIE (341050, Research Council of Finland). Publishing fees are supported by the Funding Programme Open Access Publishing of Hamburg University of Technology (TUHH).

References

1. O. Verschatse, L. Daelemans, W. V. Paepegem, and K. de Clerck, "In-Situ Observations of Microscale Ductility in a Quasi-Brittle Bulk Scale Epoxy," *Polymers* 12, no. 11 (2020): 2581, https://doi.org/10.3390/polym12112581.

2. T. J. Vaughan and C. T. McCarthy, "Micromechanical Modelling of the Transverse Damage Behaviour in Fibre Reinforced Composites," *Composites Science and Technology* 71 (2011): 388–396, https://doi.org/10.1016/j.compscitech.2010.12.006.

3. W. Tan, F. Naya, L. Yang, et al., "The Role of Interfacial Properties on the Intralaminar and Interlaminar Damage Behaviour of Unidirectional Composite Laminates: Experimental Characterization and Multiscale Modelling," *Composites Part B: Engineering* 138 (2018): 206–221, https://doi.org/10.1016/j.compositesb.2017.11.043.

4. M.-F. Ren, X.-W. Zhang, C. Huang, B. Wang, and T. Li, "An Integrated Macro/Micro-Scale Approach for In Situ Evaluation of Matrix Cracking in the Polymer Matrix of Cryogenic Composite Tanks," *Composite Structures* 216 (2019): 201–212, https://doi.org/10.1016/j.compstruct.2019.02.079.

5. X. M. Sui, I. Pinkas, and H. D. Wagner, "A Polarized Micro-Raman Study of Necked Epoxy Fibers," *Polymer* 230 (2021): 124034, https://doi.org/10.1016/j.polymer.2021.124034.

6. X. M. Sui, M. Tiwari, I. Greenfeld, et al., "Extreme Scale-Dependent Tensile Properties of Epoxy Fibers," *eXPRESS Polymer Letters* 13, no. 11 (2019): 993–1003, https://doi.org/10.3144/expresspolymlett.2019.86.

7. J. Mittelhaus, S. P. Bhusare, N. Pournoori, et al., "Understanding the Scale Dependent Ductility of Epoxies," *ECCM21—21th European Conference on Composite Materials* 2 (2024): 300–307, https://doi.org/10.60691/yj56-np80.

8. J. Mittelhaus, P. Röttger, E. Schill, J. Jacobs, and B. Fiedler, "Investigation of the Ductile Deformation Potential of Microscale Epoxy Materials," *Polymer Testing* 128 (2023): 108217, https://doi.org/10.1016/j.polymertesting.2023.108217.

9. A. Jelić, M. Sekulić, M. Travica, et al., "Determination of Mechanical Properties of Epoxy Composite Materials Reinforced With Silicate Nanofillers Using Digital Image Correlation (Dic)," *Polymers* 14 (2022): 1255, https://doi.org/10.3390/polym14061255.

10. J. J. Andrew, V. Arumugam, D. J. Bull, and H. N. Dhakal, "Residual Strength and Damage Characterization of Repaired Glass/Epoxy Composite Laminates Using a.e. and d.i.c," *Composite Structures* 152 (2016): 124–139, https://doi.org/10.1016/j.compstruct.2016.05.005.

11. Z. Jin, S. Li, H. Song, Z. Li, and D. Zhu, "Experimental and Simulative Study of Bonding Properties on Fiber/Epoxy Interfaces by Digital Image Correlation (Dic) Technique and Molecular Dynamics," *Cement and Concrete Composites* 131 (2022): 104569, https://doi.org/10.1016/j.cemconcomp.2022.104569.

12. K. Naresh, K. Shankar, R. Velmurugan, and N. K. Gupta, "High Strain Rate Studies for Different Laminate Configurations of Bi-Directional Glass/Epoxy and Carbon/Epoxy Composites Using Dic," *Structure* 27 (2020): 2451–2465, https://doi.org/10.1016/j.istruc.2020.05.022.

13. A. T. Owens and H. V. Tippur, "Measurement of Mixed-Mode Fracture Characteristics of an Epoxy-Based Adhesive Using a Hybrid Digital Image Correlation (Dic) and Finite Elements (Fe) Approach," *Optics and Lasers in Engineering* 140 (2021): 106544, https://doi.org/10.1016/j.optlaseng.2021.106544.

14. S. Zike, B. F. Sørensen, and L. P. Mikkelsen, "Experimental Determination of the Micro-Scale Strength and Stress-Strain Relation of an Epoxy Resin," *Materials & Design* 98 (2016): 47–60, https://doi.org/10.1016/j.matdes.2016.02.102.

15. D. I. Bower, "Investigation of Molecular Orientation Distributions by Polarized Raman Scattering and Polarized Fluorescence," *Journal of Polymer Science: Polymer Physics Edition* 10 (1972): 2135–2153, https://doi.org/10.1002/pol.1972.180101103.

16. D. I. Bower, "Raman Scattering From an Assembly of Partially Oriented Scatterers," *Journal of Physics B: Atomic and Molecular Physics* 9 (1976): 3275–3293, https://doi.org/10.1088/0022-3700/9/18/018.

17. B. Jasse and J. L. Koenig, "Orientational Measurements in Polymers Using Vibrational Spectroscopy," *Journal of Macromolecular Science, Part C: Polymer Reviews* 17 (1979): 61–135, https://doi.org/10.1080/00222357908080905.

18. B. Jasse and J. L. Koenig, "Polarized Raman Study of Molecular Orientation in Uniaxially Stretched Atactic Polystyrene," *Journal of Polymer Science: Polymer Physics Edition* 18 (1980): 731–738, https://doi.org/10.1002/pol.1980.180180406.

19. L. Svenningsson and L. Nordstierna, "Polarized Raman Spectroscopy Strategy for Molecular Orientation of Polymeric Fibers With Raman Tensors Deviating From the Molecular Frame," *ACS Applied Polymer Materials* 2 (2020): 4809–4813, https://doi.org/10.1021/acsapm.0c00762.

20. S. Frisk, R. M. Ikeda, D. B. Chase, and J. F. Rabolt, "Determination of the Molecular Orientation of Poly(Propylene Terephthalate) Fibers Using Polarized Raman Spectroscopy: A Comparison of Methods," *Applied Spectroscopy* 58 (2004): 279–286, https://doi.org/10.1366/00037020432288661 8.

21. A. Soto, S. M. Iconomopoulou, A. C. Manikas, and G. A. Voyiatzis, "Molecular Orientation of Poly(Ethylene Terephthalate) and Poly(Butylene Terephthalate) Probed by Polarized Raman Spectra: A Parallel Study," *Applied Spectroscopy* 59 (2005): 1257–1269, https://doi.org/10.1366/000370205774430882.

22. C. Lesko, J. F. Rabolt, R. M. Ikeda, B. Chase, and A. Kennedy, "Experimental Determination of the Fiber Orientation Parameters and the

Raman Tensor of the 1614 cm^{-1} Band of Poly(Ethylene Terephthalate)," *Journal of Molecular Structure* 521, no. 1-3 (2000): 127–136, https://doi.org/10.1016/S0022-2860(99)00430-5.

23. S. Yang and S. Michielsen, "Orientation Distribution Functions Obtained via Polarized Raman Spectroscopy of Poly(Ethylene Terephthalate) Fibers," *Macromolecules* 36 (2003): 6484–6492, https://doi.org/10.1021/ma034486q.

24. M. J. Citra, D. B. Chase, R. M. Ikeda, and K. H. Gardner, "Molecular Orientation of High-Density Polyethylene Fibers Characterized by Polarized Raman Spectroscopy," *Macromolecules* 28 (1995): 4007–4012, https://doi.org/10.1021/ma00115a037.

25. X. Chen, M. A. Leugers, T. Kirch, and J. Stanley, "Orientation Mapping of Extruded Polymeric Composites by Polarized Micro-Raman Spectroscopy," *Journal of Spectroscopy* 2015 (2015): 1–7, https://doi.org/10.1155/2015/518054.

26. E. Jones and M. Iadicola, "A Good Practices Guide for Digital Image Correlation. International Digital Image Correlation Society," 2018, https://doi.org/10.32720/idics/gpg.ed1.

27. B. Fiedler, M. Hojo, S. Ochiai, K. Schulte, and M. Ando, "Failure Behavior of an Epoxy Matrix Under Different Kinds of Static Loading," *Composites Science and Technology* 61, no. 11 (2001): 1615–1624, https://doi.org/10.1016/S0266-3538(01)00057-4.

28. J. Drummer, D. Gibhardt, J. Körbelin, and B. Fiedler, "General Influence of the Environmental Temperature on the Matrix Strength Under Tensile and Compressive Loading—A Comprehensive Study on High Performance Matrices," *Composites Science and Technology* 230 (2022): 109486, https://doi.org/10.1016/j.compscitech.2022.109486.

29. H. van Melick, L. E. Govaert, and H. Meijer, "On the Origin of Strain Hardening in Glassy Polymers," *Polymer* 44 (2003): 2493–2502, https://doi.org/10.1016/S0032-3861(03)00112-5.

30. R. N. Haward, "Strain Hardening of Thermoplastics," *Macromolecules* 26 (1993): 5860–5869, https://doi.org/10.1021/ma00074a006.

31. C. Tian, R. Xiao, and J. Guo, "An Experimental Study on Strain Hardening of Amorphous Thermosets: Effect of Temperature, Strain Rate, and Network Density," *Journal of Applied Mechanics* 85 (2018): 101012, https://doi.org/10.1115/1.4040692.

32. K. W. Thomson and L. J. Broutman, "Strain Softening in an Epoxy Resin," *Journal of Materials Science* 17 (1982): 2700–2708, https://doi.org/10.1007/BF00543907.

33. A. F. Betancur, A. García, and F. R. Pérez, "Thermal Stability and Chemical Analysis of Hybrid Materials Reinforced With Graphene Oxide," *Journal of Physics: Conference Series* 1219 (2019): 012003, https://doi.org/10.1088/1742-6596/1219/1/012003.

34. R. E. Lyon, K. E. Chike, and S. M. Angel, "In Situ Cure Monitoring of Epoxy Resins Using Fiber–Optic Raman Spectroscopy," *Journal of Applied Polymer Science* 53, no. 13 (1994): 1805–1812, https://doi.org/10.1002/app.1994.070531310.

35. X. Liao, M. Dulle, E. S. Souza, et al., "High Strength in Combination With High Toughness in Robust and Sustainable Polymeric Materials," *Science* 366 (2019): 1376–1379, https://doi.org/10.1126/science.aay9033.

36. P. Larkin, *Infrared and Raman Spectroscopy: Principles and Spectral Interpretation*, 2nd ed. (Elsevier, 2018), https://doi.org/10.1016/C2015-0-00806-1.

37. P. Laurikainen, S. Bhusare, G. Mohanty, and E. Sarlin, "Length-Scale Discrepancy in the Properties of Epoxy Resin Specimens," *Polymer* 283 (2023): 126148, https://doi.org/10.1016/j.polymer.2023.126148.

Supporting Information

Additional supporting information can be found online in the Supporting Information section.